Analysis of the Uniform Rate Equation Model of Laser Dynamics

THOMAS J. MENNE

Abstract—The spatially independent laser rate equation model is generalized to include multimode effects, and it is also shown that the same description of laser behavior as provided by the single-mode model results. Analytical expressions for the steady-state values of the variables in all modes are derived. It is shown that a singularity at the oscillation threshold exists in the steady-state equations which is responsible for the laser action. It is further demonstrated that the inverted population and the photon density in off-axis modes saturates above threshold, whereas the photon density in the primary mode increases linearly with pump rate above threshold. The exact time-dependent solutions are determined numerically, and it was found that the spiking separation and decay time could change by more than 50 percent of their values at the start of laser emission to the region of steady-state oscillation, even when the pump is assumed to be time independent. The linearized expressions for the spiking parameters are, therefore, inadequate—despite their frequent use—to describe phenomena appearing in the early portions of the spiking trace. A comparison with five experimental cases is also made. It was found that this model, with all modes included, provides no improvement over the single mode model, and cannot account for the irregular or undamped spiking or even the multimode oscillations observed experimentally.

I. Introduction

THE RATE EQUATION model has been widely used [1]–[12] to describe the relaxation oscillations or spikes observed [13]–[16] in the power output of lasers. Single mode analyses in particular have been conducted, and because of their simplicity, have been frequently used to predict spiking characteristics for a given set of experimental conditions. The validity of such a model is questionable, however, since most lasers exhibit multimode oscillations. It would seem reasonable, therefore, to extend the familiar rate equation model by including those modes lying near the center of the fluorescent line and coupled to each other through the inverted electron population. This model is not as general as that of Tang, Statz, and de Mars [9] who consider the coupling produced by the spatial dependence of the photon and electron populations, but it has the advantage of retaining the simplicity of the original model so that it is amenable to non-numerical solution. In addition, the modifications, if any, of the single mode spiking behavior produced by a natural extension of the same model help to determine the range of validity of the original model itself.

Manuscript received September 13, 1965; revised November 12, 1965.

The author is with the McDonnell Aircraft Corporation, St. Louis, Mo.

II. Rate Equations

Let u_i be the number of photons of frequency ν_i in the ith cavity mode, and $n = n_2 - n_1$ be the electron population difference between the upper and lower laser levels. The analysis will be confined to three-level systems, such as ruby, although with the proper redefinition of the parameters [17], it is also applicable to four-level lasers. When u_i and n are normalized by $N_0 = n_1 + n_2$, the rate equations may be written

$$\dot{u}_i = -\alpha_i u_i + B_i N_0 n u_i + \frac{B_i}{2}(n+1) \qquad (i = 1, \cdots p) \tag{1}$$

$$\dot{n} = -(W + A)n - 2n \sum_{i=1}^{p} B_i N_0 u_i + (W - A), \tag{2}$$

where $A = \tau^{-1}$, and τ is the fluorescent lifetime of the upper laser level; W is the optical pumping rate and is assumed to be time independent; α_i is the rate of loss of photons from the ith mode; B_i is the transition probability per photon in the ith mode; and p is the total number of cavity modes within the fluorescent linewidth.

The principal loss mechanisms for photons are scattering, diffraction, and transmission through the end mirrors; and the total loss rate α_i is the sum of these individual loss rates. The transmission loss rate α_T is given by:

$$\alpha_T = -\frac{c}{n_r L} \ln \sqrt{R_1 R_2}, \tag{3}$$

where c is the velocity of light, R_1 and R_2 are the reflection coefficients of the end faces, n_r is the index of refraction for ruby, and L is the cavity length. Campbell and Van Nest [18] indicate that scattering and diffraction can each remove 20 percent of the photon population per pass. However, these losses will not be considered explicitly here, since they affect only the magnitude of α_i and not the form of (1).

The transition probability for stimulated emission in the ith cavity mode is given by [19]

$$B_i = \frac{A}{p} \frac{(\Delta\nu)^2}{(\nu_i - \nu_0)^2 + (\Delta\nu)^2} \tag{4}$$

for a fluorescent line of Lorentzian shape with center frequency ν_0 and half-width $\Delta\nu$, and the number of cavity modes p is given by [19]

$$p = 8\pi^2\nu_0^2 n_r^3 \Delta\nu V/c^3, \tag{5}$$

where V is the cavity volume.

The various modes are characterized by only two parameters, α_i and B_i. Modes with the same longitudinal mode number and only slightly different transverse mode numbers are nearly degenerate; their frequencies ν_i and, hence, their values of B_i are approximately equal. Thus, differences between these modes manifest themselves primarily in the loss rate parameters α_i, which may differ by as little as one part in 10^3.

Lasers exhibit an oscillation threshold which is defined as the minimum value of the inverted population n_t, for which the rate of gain of the coherent radiation balances the loss rate. Thus, equating the first two terms of (1) yields

$$n_t = \alpha_1/B_1N_0, \tag{6}$$

where the subscript 1 refers to the primary axial mode, identified as the mode possessing the minimum loss rate α_1, maximum stimulated emission rate B_1, and mode frequency $\nu_1 = \nu_0$.

III. Steady State

A. Single Mode Analysis

Equations (1) and (2) constitute a set of $p + 1$ first order, nonlinear, coupled differential equations. Their behavior can best be understood by first considering the particular case of single mode operation, where only the primary axial mode $i = 1$ is present. Then (1) and (2) reduce to two equations in u_1 and n:

$$\dot{u}_1 = -\alpha_1 u_1 + B_1N_0 n u_1 + \frac{B_1}{2}(n + 1) \tag{7}$$

$$\dot{n} = -\beta_+ n - 2B_1N_0 n u_1 + \beta_-, \tag{8}$$

where

$$\beta_\pm = W \pm A. \tag{9}$$

The steady-state solutions, denoted by the subscript s and obtained by setting $\dot{u}_1 = \dot{n} = 0$, are given by

$$u_{1s} = \frac{\frac{B_1}{2}(n_s + 1)}{\alpha_1 - B_1N_0 n_s}, \tag{10}$$

and

$$n_s = \frac{\beta_-}{\beta_+ + 2B_1N_0u_{1s}}. \tag{11}$$

Some insight into the transient behavior and the steady-state solutions can be obtained from a phase plane analysis of u_1 and n. For this purpose, the relation

$$\frac{du_1}{dn} = \frac{-\alpha_1 u_1 + B_1N_0 n u_1 + \frac{B_1}{2}(n + 1)}{-\beta_+ n - 2B_1N_0 n u_1 + \beta_-} \tag{12}$$

is formed.

Figures 1 and 2 are phase plane diagrams for $\beta_-/\beta_+ > n_t$ and $\beta_-/\beta_+ < n_t$, respectively. The plot of (10) gives the locus of points where the numerator of (12) vanishes, and the plot of (11) is the locus of points where the denominator of (12) vanishes. The intersection of the two solid curves is the only physical singularity or stability point of the system. The $(\pm)$ signs represent the sign of (12) ,which gives the slope of the solution curves. Any solution curve crossing the curve of (10) must have zero slope, and any solution curve crossing the curve of (11) must have infinite slope. Only the region of physical interest, $u_1 > 0$, $-1 < n < 1$ is shown, and the dashed curves in Figs. 1 and 2 are the solution curves for the

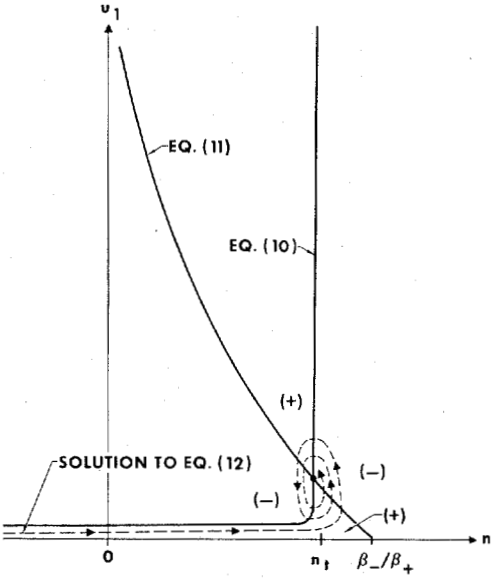

Fig. 1. Phase plane diagram for the single mode ruby laser when $\beta_-/\beta_+ > n_t$.

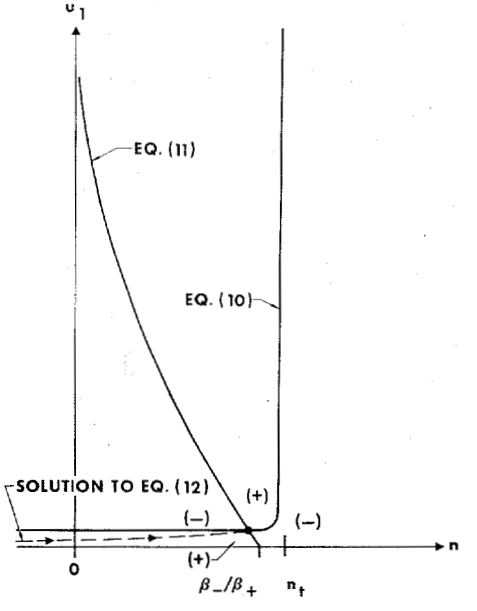

Fig. 2. Phase plane diagram for the single mode ruby laser when $\beta_-/\beta_+ < n_t$.

initial conditions $u_1(0) = 0$, $n(0) = -1$. The arrows indicate the direction of increasing time.

It can be seen from Fig. 1 that as n reaches and exceeds the value n_t, u_1 increases by orders of magnitude and then executes a damped, oscillatory motion, suggesting spiking behavior, about the stability point.

Now consider Fig. 2, where $\beta_-/\beta_+ < n_t$. From (8) it is clear that if there is no electromagnetic radiation ($u_1 = 0$), then n approaches the value β_-/β_+ exponentially. The presence of radiation in the cavity only serves to drive n down when n is positive. Thus, β_-/β_+ is the maximum value attainable by n, so that if $\beta_-/\beta_+ < n_t$, the solution curve in Fig. 2 can neither climb to large values of u_1 nor execute oscillations about the singularity without violating the conditions for slopes discussed above and indicated in Fig. 2. Consequently, the threshold pump rate W_t is determined by the condition $(\beta_-/\beta_+)_t = n_t$, or

$$W_t = A\left(\frac{1 + n_t}{1 - n_t}\right). \tag{13}$$

The simultaneous equations (10) and (11) possess a singularity at the point $n_s = n_t = \alpha_1/B_1N_0$, such that if $n_s = n_t$, then $u_{1s} = \infty$; and if $n_s > n_t$, then $u_{1s} < 0$. But the phase plane diagrams show that steady-state solutions in the physically admissible region $u_{1s} > 0$ never reach the singularity point $n_s = n_t$. This can be seen in the following way: when $\beta_-/\beta_+ < n_t$, i.e., $W < W_t$, then u_{1s} [as given by (10)] has a negligibly small value, since the numerator is the spontaneous emission term, and the denominator has a large nonzero value. Consequently, from (11), $n_s \approx \beta_-/\beta_+$ to a high degree of approximation. However, when $\beta_-/\beta_+ \geq n_t$, i.e., $W \geq W_t$, then n_s approaches arbitrarily close to the value n_t and u_{1s} increases by orders of magnitude from its prethreshold value. Then the second term in the denominator of (11) becomes comparable with the first and serves to maintain the difference $(n_t - n_s)$ infinitesimally small and positive.

Although (10) is rigorously correct for $W \geq W_t$, it is not analytically tractable; and an expression for u_{1s} can be more readily obtained from (11) by setting $n_s \approx n_t$:

$$u_{1s} \approx \frac{1}{2\alpha_1}(\beta_- - n_t\beta_+). \tag{14}$$

Note that u_{1s} is linear in the pump rate W above threshold.

B. Multimode Analysis

With the help of the results from the single mode case, the multimode rate equations (1) and (2) can now be treated. Their steady-state solutions are

$$n_s = \beta_-\left\{\beta_+ + 2\sum_{i=1}^{p} B_iN_0u_{is}\right\}^{-1}, \tag{15}$$

and

$$u_{is} = \frac{B_i}{2}(n_s + 1)\{\alpha_i - B_iN_0n_s\}^{-1}. \tag{16}$$

Below threshold, the photon populations in all modes are generated by spontaneous emission, as given by (16), and, therefore, will be small. Thus,

$$\left.\begin{aligned} &n_s \approx \frac{\beta_-}{\beta_+}, \qquad (17)\\ &\text{and}\\ &u_{is} \approx \frac{B_i}{2}\left(\frac{\beta_-}{\beta_+} + 1\right)\left\{\alpha_i - B_iN_0\frac{\beta_-}{\beta_+}\right\}^{-1}, \qquad (18)\end{aligned}\right\} \quad (W < W_t)$$

for all $i = 1, \cdots p$.

Above threshold, it was found from the single mode analysis that n_s cannot exceed $n_t = \alpha_1/B_1N_0$. But since $\alpha_1/B_1N_0 < \alpha_i/B_iN_0$ for all $i = 2, \cdots p$, it follows that it is impossible to reach threshold in the steady state for all modes $i \neq 1$. Consequently, the u_{is} $(i \neq 1)$ given by (16) will remain small with respect to u_{1s} and may be dropped from the sum in (15). Thus, an expression for u_{1s} can be obtained from (15) in the same manner as the single mode case, with the result

$$\left.\begin{aligned} &n_s \approx n_t, \qquad (19)\\ &u_{is} \approx \frac{B_i}{2}(n_t + 1)\{\alpha_i - B_iN_0n_t\}^{-1}, \quad i \neq 1 \qquad (20)\\ &u_{1s} \approx \frac{1}{2\alpha_1}(\beta_- - n_t\beta_+). \qquad (21)\end{aligned}\right\} (W \geq W_t).$$

It can be seen from (19) and (20) that the inverted population remains constant at its threshold value and that the steady-state values of the photon populations are independent of W in all modes except the dominant mode. In contrast to this behavior, the steady-state primary mode photon population u_{1s}, given by (21), increases linearly with the pump rate W.

One of the shortcomings of the simplified rate equation model is already apparent, viz., that only the dominant mode can reach oscillation threshold in the steady state. This is in disagreement with the observed multimode performance of most solid-state lasers.

Equations (17) through (21) provide analytical expressions for the steady-state inverted population and photon density for a multimode ruby laser both below and above threshold in terms of measurable quantities. As a check on the approximations used in arriving at the above expressions, the cubic equation that results from the simultaneous solutions of (15) and (16) for a two-mode case was solved numerically. The results are shown in Figs. 3 and 4 which are plots of u_{1s}, u_{2s}, and n_s as a function of the pump rate W. The parameters are those associated with a ruby laser rod at room temperature, where $A = 330\ s^{-1}$. Its length is 3 inches; diameter, $\frac{3}{8}$ inch; chromium concentration, 0.02 percent by weight; and average reflectivity, 95 percent. We take $\lambda_0 = 6943$ Å, $n_r = 1.76$, $B_2 = B_1$, and $\alpha_2 = 1.01\alpha_1$.

The values shown in Figs. 3 and 4 agree with those

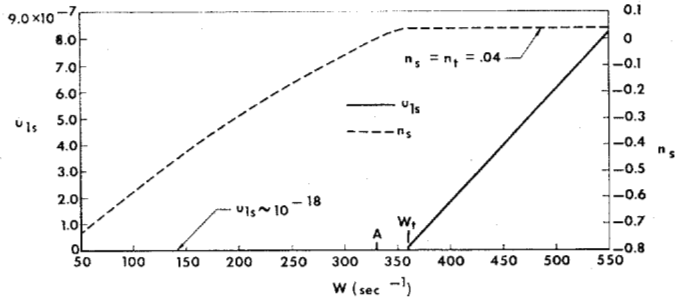

Fig. 3. Plot of u_{1s} and n_s against W for the two mode ruby laser.

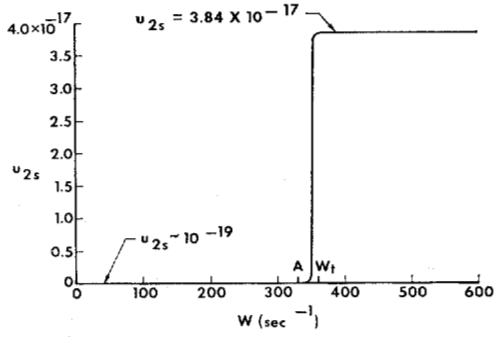

Fig. 4. Plot of u_{2s} vs. W for the two mode ruby laser.

determined from the analytical expressions within one part in 10^6 for both $W < W_t$ and $W \geq W_t$ and thus confirm the validity of the approximations. The quantity u_{1s} increases by ten orders of magnitude as the threshold is crossed and is linear thereafter; u_{2s} increases by only 10^2 and remains constant above the threshold point; and n_s does not exceed the value n_t. These results corroborate the predictions stated above. It is also seen that u_{2s}/u_{1s} is of the order of 10^{-10}, so that the approximation $u_{2s} \ll u_{1s}$ used in arriving at (21) is well-founded. Note that, although the equations describing the two modes are identical (except that $\alpha_2 = 1.01\ \alpha_1$), their solutions have a grossly different behavior.

IV. Spiking Characteristics

The spiking characteristics predicted by the rate equation model will first be determined for the single mode case. Then a second mode, lying spectrally near the first, will be added in order to study its effect on the former results.

Spiking behavior in the region of the stability point may be examined by expanding u_1 and n about their steady-state values u_{1s} and n_s. For the range of pump values $W \geq W_t$ and for the single mode case $n_s = n_t$ and $u_{1s} = (\beta_- - n_t\beta_+)/2\alpha_1$, as given by (19) and (21), respectively. Let

$$u_1 = u_{1s} + x_1, \qquad n = n_t + y, \tag{22}$$

where $x_1 \ll u_{1s}$ and $y \ll n_t$. Near steady-state operation, the spontaneous emission term in (7) can be dropped, as is indicated by the large values of u_1 implied by the phase plane diagram of Fig. 1 and the analysis of the preceding section. Then x_1 and y satisfy

$$\dot{x}_1 = Ox_1 + B_1N_0u_{1s}y \tag{23}$$

$$\dot{y} = -2B_1N_0n_tx_1 - \frac{\beta_-}{n_t}y, \tag{24}$$

to first order in x_1 and y. The secular equation is

$$s^2 + \frac{\beta_-}{n_t}s + 2(B_1N_0)^2n_tu_{1s} = 0, \tag{25}$$

and its solutions are

$$s = -\frac{1}{\tau_d} \pm i\omega, \tag{26}$$

where

$$\tau_d = 2n_t/\beta_-, \tag{27}$$

and

$$\omega = \{\alpha_1(\beta_-/n_t - \beta_+) - (\beta_-/2n_t)^2\}^{1/2} \tag{28}$$

$$\approx \{\alpha_1(\beta_-/n_t - \beta_+)\}^{1/2}, \tag{29}$$

since $\beta_-/2n_t \ll \alpha_1$.

An interesting feature of (28) is that it predicts an upper cutoff value W_m beyond which there is no spiking. Setting $\omega = 0$ yields a quadratic equation in W with the two solutions $W_m = W_t$, as expected, and

$$W_m \approx A + 4n_t\alpha_1(1 - n_t) \approx 4n_t\alpha_1(1 - n_t). \tag{30}$$

To suppress spiking in a typical ruby laser, a pump ratio $W_m/W_t \approx 10^4$ would be required, which is probably not practical.

Now consider two-mode laser action for $W \geq W_t$. If the analysis is carried forward in the same manner as for the single mode case, the following cubic secular equation is obtained:

$$s^3 + s^2(\alpha_2 - \alpha_1 + \beta_-/n_t) + s\left[\frac{\beta_-}{n_t}(\alpha_2 - \alpha_1) + 2(B_1N_0)^2n_t(u_{1s} + u_{2s})\right] + 2(B_1N_0)^2n_tu_{1s}(\alpha_2 - \alpha_1) = 0. \tag{31}$$

As was shown above, however, $u_{2s} \ll u_{1s}$, so that the u_{2s} term in the coefficient of s may be dropped. Then (31) factors into a product of a linear and a quadratic expression in s. The root s_3 of the linear equation is

$$s_3 = -(\alpha_2 - \alpha_1). \tag{32}$$

If $B_2 \neq B_1$, (32) becomes

$$s_3 = -\left(\alpha_2 - \frac{B_2}{B_1}\alpha_1\right). \tag{33}$$

The other roots $s_{1,2}$ satisfy the quadratic equation

$$s_{1,2}^2 + \frac{\beta_-}{n_t}s_{1,2} + 2(B_1N_0)^2n_tu_{1s} = 0, \tag{34}$$

which is identical with (25) of the single mode case. Consequently, the spiking frequency (28) and decay time (27) are the same. Numerical values for these quantities have also been determined from computer solutions of (31) over a range of pump rates W, and agreement with values obtained from (27), (28), and (33) was found within one part in 10^6.

It appears, therefore, that the net effect of the second mode is to introduce a pure decay constant s_3, which becomes larger the greater the ratio $\alpha_2 B_1/\alpha_1 B_2$, and which is chiefly effective in the second mode. The same spiking frequency is expected for both u_1 and u_2, although they may be phase shifted relative to one another. Consequently, the simple rate equation model, even when modified to include multimode operation, does not explain the irregular spiking frequently observed in laser outputs.

Laser action in more than two modes is not analyzed here in detail because these other modes must necessarily be even further removed from the primary mode u_1, and consequently, should have an even smaller effect on the spiking behavior.

In order to evaluate the model further, a comparison was made between the theoretical spiking results and experimental data reported in the literature. The two-mode analysis with $\alpha_2 = 1.01\alpha_1$ and $B_2 = B_1$ was used in each case. The quantity α_1 was computed from (3). All the necessary pertinent data (temperature, cavity geometry, reflectivity, chromium concentration, pump-to-threshold ratio) were available in only three of the five cases studied. Thus, it was necessary to make reasonable estimates for the values of the missing quantities. In addition, it was necessary to multiply (3) by the ratio $1350/2030 = 0.66$ for Case 4 in order to adjust for the confocal mirrors.

The linearized spiking period $T = 2\pi/\omega$ and the decay constant τ_d are given in Table I together with their observed values, where measured. Note that a finite value of τ_d is reported only for Case 3 and that the predicted value differs by approximately 35 percent. The differences between the observed and computed values of the spiking period are 1.6, 1.5, 1.2, 0.1, and 2.3 μs, so that a fair degree of agreement between theory and experiment is obtained.

TABLE I
THEORETICAL AND EXPERIMENTAL VALUES OF THE SPIKING PERIOD T AND DECAY CONSTANT τ_d

Investigator	W/W$_t$	Theoretical		Experimental	
		$T(\mu s)$	$\tau_d(\mu s)$	$T(\mu s)$	$\tau_d(\mu s)$
Maiman et al. [20]	2.00	4.1	206	~2.5	*
Collins et al. [13]	1.40*	6.5	130	~5	*
Gerber et al. [21]	1.55	7.7	45	6.5	69
Johnson et al. [22]	2.37	3.6	27.8	3.5	*
Nelson and Boyle [15]	1.20	8.9	642	~6.6	∞

*Not reported

Case 5 represents the experiment of Nelson and Boyle [15], in which a ruby laser was operated continuously and maintained at liquid nitrogen temperature, so that the assumptions of a CW pump and a constant fluorescent lifetime are satisfied. The most significant result of that experiment was the absence of an observable decay of the spiking envelope. But (27) shows that the decay rate τ_d^{-1} will never vanish identically. Moreover, the phase plane diagram of Fig. 1 does not admit to a limit cycle as a possible solution curve, as has also been shown by Makhov [4]. Nelson and Boyle state that the losses in the crystal are probably much larger than the transmission losses, so that a high degree of mode coupling may be expected. The simple model considered here does not include these effects, and so, not surprisingly, does not predict undamped spiking.

Gürs [23] has recently observed damped spiking and nearly constant output by reducing losses through the use of a long cavity. It can be shown from (27) that, over some range of the total loss rate, the decay constant τ_d decreases as the losses decrease, provided W/W_t remains constant. Hence, the experimental results of Gürs provide some confirmation of this model.

As a further check on the spiking results obtained above by expansion about the steady-state values of the variables, the time-dependent solutions of the two-mode rate equations were determined by direct numerical integration. They are presented in Figs. 5 and 6, using, for illustrative purposes only, values of the rate equation parameters appropriate to the Nelson and Boyle [15] case; $t = 0$ is arbitrary and represents the start of laser action. The mode u_2 is characterized by the values $B_2 = B_1$ and $\alpha_2 = 1.001\alpha_1$.

It can be seen from Figs. 5 and 6 that the decay time and spiking period are not constant even under the assumed time-independent pumping conditions, although they are smoothly varying functions of time which eventually approach their predicted values near the steady state. An even more complicated variation in these quantities is therefore expected in pulsed operation. In addition, it can be seen that the deviation of u_1 and u_2 from their steady-state values u_{1s} and u_{2s} is sufficiently great to render a first order expansion meaningless near the start of oscillations.

These two phenomena indicate that the good agreement obtained between the predicted and observed values of the spiking period in Table I may be fortuitous. It is suggested that this agreement resulted from underestimating system losses, since only transmission losses were considered. Values of T computed from (29) would then be too large and would more nearly approximate the values near the start of laser oscillation, where the spiking periods were measured. To calculate or even estimate scattering and diffraction losses for a given laser, however, is exceedingly difficult; and their values were not recorded in the literature for the cases considered in Table I.

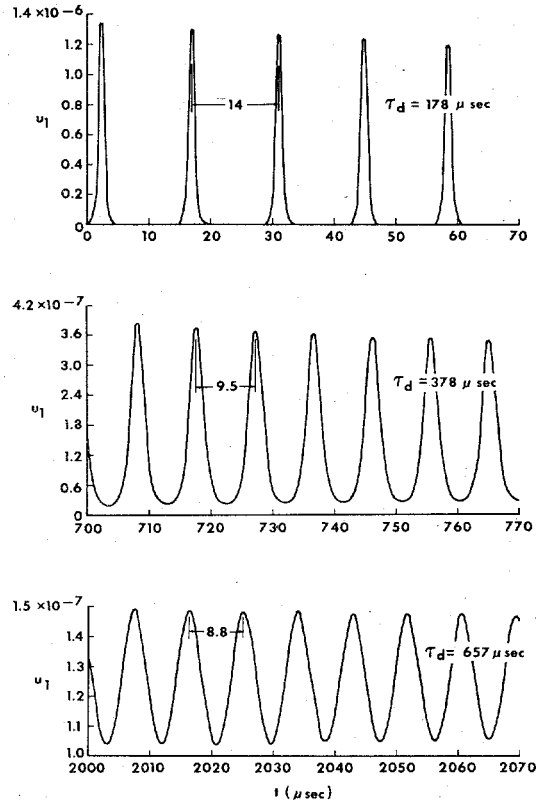

Fig. 5. Plot of the temporal behavior of u_1 for Case 5 of Table I. The steady-state value of u_{1s} is 1.23×10^{-7}.

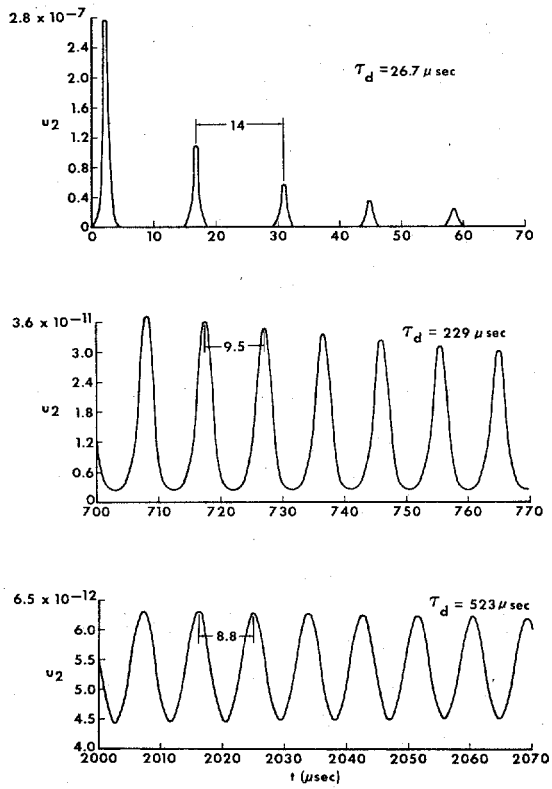

Fig. 6. Plot of the temporal behavior of u_2 for Case 5 of Table I. The steady-state value of u_{2s} is 5.25×10^{-12}.

V. Conclusions

The simple space-independent rate equation model so often used in the description of laser dynamics was studied in detail. It was found that, even when multimode operation is explicitly included, this model fails to account for irregular or undamped spiking, as well as multimode oscillations in the steady state. These phenomena are described by the model of [9] and [11], however.

The assumption of a time-independent pump rate W is not considered to be the primary shortcoming of the model, since it is only necessary that W remain constant for a time long compared with a spiking period in order that the spiking description be meaningful. This condition is usually satisfied even under pulsed operation. It was shown in Section IV that the expressions for the spiking parameters T and τ_d obtained from the linearized solutions of the rate equations generally provided a poor description of spiking characteristics near the start of laser action, and that a more reliable description could be obtained only from the numerical solution of the full rate equations. Since the advantage of simplicity of this model would then be lost, another, more realistic approach should then be pursued, preferably, the density matrix model of Fleck and Kidder [24], which provides for direct mode coupling.

Acknowledgment

The author would like to express his appreciation to Drs. D. P. Ames, J. G. Boerman, J. E. Dueker, C. D. Gorman, and F. J. Rosenbaum for many stimulating discussions and helpful suggestions on a variety of aspects of this work. He would also like to acknowledge J. Whitesell for his competent and efficient computer programming, without which this research would have been greatly delayed.

References

[1] H. Statz, and G. de Mars, "Transient and oscillation pulses in masers," in *Quantum Electronics*. New York: Columbia U. P., 1960, pp. 530–537.
[2] H. Statz, C. Luck, C. Shafer, and M. Ciftan, "Observations on oscillation spikes in multimode lasers," in *Advances in Quantum Electronics*. New York: Columbia U. P., 1961, pp. 342–347.
[3] R. Dunsmuir, "Theory of relaxation oscillations in optical masers," *J. Electronics and Control (GB)*, vol. 10, 453–458, 1961.
[4] G. Makhov, "On the problem of pulsed oscillations in ruby masers," *J. Appl. Phys.*, vol. 33, pp. 202–204, January 1962.
[5] E. J. Post, "Threshold and stability of a simplified model optical maser," *Appl. Opt.*, vol. 1, pp. 165–168, March 1962.
[6] K. Shimoda, "Amplitude and frequency variations in ruby optical masers," *Proc. of the Symposium on Optical Masers*. New York: Polytechnic Press, 1963, pp. 95–108.
[7] M. Birnbaum, T. Stocker, and S. J. Welles, "Pulsed oscillations in ruby lasers," *Proc. IEEE (Correspondence)*, vol. 51, pp. 854–855, May 1963.
[8] J. I. Kaplan, "Criterion for continuous amplitude oscillations of optical masers," *J. Appl. Phys. (Communications)*, vol. 34, pp. 3411–3412, November 1963.
[9] C. L. Tang, H. Statz, and G. de Mars, "Spectral output and spiking behavior of solid-state lasers," *J. Appl. Phys.*, vol. 34, pp. 2289–2295, August 1963.
[10] W. W. Clendenin, "Large-amplitude solutions of the rate

equations for the ruby laser," *J. Appl. Phys.*, vol. 35, pp. 2277–2278, August 1964.
[11] H. Statz, and C. L. Tang, "Multimode oscillations in solid-state lasers," *J. Appl. Phys.*, vol. 35, pp. 1377–1383, May 1964.
[12] D. D. Bhawalkar, W. A. Gambling, and R. C. Smith, "Investigation of relaxation oscillations in the output from a ruby laser," *The Radio and Electronics Engineer*, vol. 27, pp. 285–291, April 1964.
[13] R. J. Collins, D. F. Nelson, A. L. Schawlow, W. Bond, C. G. B. Garrett, and W. Kaiser, "Coherence, narrowing, directionality, and relaxation oscillations in the light emission from ruby," *Phys. Rev. Leters*, vol. 5, pp. 303–305, October 1960.
[14] P. P. Sorokin, and M. J. Stevenson, "Stimulated emission from *Ca* F_2: U^{+3} and *Ca* F_2: Sm^{+2}," in *Advances in Quantum Electronics*. New York: Columbia U. P. 1961, pp. 65–76.
[15] D. F. Nelson, and W. S. Boyle, "A continuously operating ruby optical maser," *J. Appl. Opt.*, vol. 1, pp. 181–183, March 1962.
[16] E. Bernal, J. F. Ready, and D. Chen, "Oscillatory character of Ca WO_4: Nd^{3+} laser output," *Proc. IEEE (Correspondence)*, vol. 52, pp. 710–711, June 1964.
[17] G. Birnbaum, *Optical Masers*. New York: McGraw-Hill, 1964, pp. 51–56.
[18] C. K. Campbell, and J. P. Van Nest, "The effects of scatter and diffraction on the spiking period of a ruby laser," *Proc. IEEE (Correspondence)*, vol. 52, pp. 210–211, February 1964.
[19] P. P. Sorokin, "Theory of four-level solid state lasers," IBM Corp., Yorktown Heights, New York, Research Rept. RC-927, May 1963.
[20] T. H. Maiman, R. H. Hoskins, I. J. D'Haenens, C. K. Asawa, and V. Evtuhov, "Stimulated optical emission in fluorescent solids. II. Spectroscopy and stimulated emission in ruby," *Phys. Rev.*, vol. 123, pp. 1151–1157, August 1961.
[21] E. A. Gerber, and E. R. Ahlstrom, "Ruby laser with piezoelectrically excited vibrating reflector," *J. Appl. Phys.*, vol. 35, pp. 2546–2547, August 1964.
[22] R. E. Johnson, W. H. McMahan, F. J. Oharek, and A. P. Sheppard, "A ruby laser exhibiting periodic relaxation oscillations," *Proc. IRE (Correspondence)*, vol. 49, pp. 1942–1943, December 1961.
[23] K. Gürs, "Beats and modulation in optical ruby-masers," in *Quantum Electronics*. New York: Columbia U. P., 1964, pp. 1113–1119.
[24] J. A. Fleck, and R. E. Kidder, "Coupled mode laser oscillation," *J. Appl. Phys.*, vol. 35, pp. 2825–2831, October 1964.

Polarization Selection for Reconstructed Wavefronts and Application to Polarizing Microholography

W. H. CARTER, MEMBER, IEEE, P. D. ENGELING, AND A. A. DOUGAL, SENIOR MEMBER, IEEE

Abstract—**This article reports a phenomenon allowing the phase reference beam of the "two-beam, carrier-frequency" holography method of Leith and Upatnieks to be used as a polarization reference as well. A technique for utilizing this for selecting and recording a particular linearly polarized component of the image carrying beam is described and applied to a unique arrangement for microholography. The waves reconstructed by the technique are described mathematically and compared to waves passed by a polarizing microscope. Experimental confirmation of these observations is presented.**

GABOR'S technique [1] for reconstructing wavefronts has been successfully demonstrated for lensless bright-field microscopy [2] in which it offers the possibility of at least two important advantages over the conventional lens system. The hologram permanently records the three-dimensional specimen rather than the usual two dimensions of a conventional photomicrograph which is limited by narrow depth of field. In lensless systems, the resolution limit imposed by the numerical aperture of the objective is replaced by that imposed by the size and resolution of the hologram plate [3].

This technique can be extended directly to dark-field and phase contrast microscopy by the use of suitable reconstructing lenses, beam splitters, and phase plates. However, the extension to the polarizing microscope is complicated by the loss of polarization information in the photographic process. This article reports an observation which realizes this for the polarizing microscope.

In the "two-beam, carrier-frequency" method first demonstrated by Leith and Upatnieks [4], a reference beam is utilized to preserve phase information and to remove a sign ambiguity. In this work, in addition, the reference beam is exploited as a polarization reference. The linearly polarized beam from a gas laser with Brewster angle windows was used as a source. In the interference process which produces the hologram, only the component of the signal beam which is polarized in the same direction as the reference beam is recorded.

Thus, when a birefringent crystal is examined where the scattered light in the signal beam contains a range of polarization components, any particular linearly polarized component can be selected by suitably rotating the polarization of the reference beam with wave plates. This serves as an analyzer, like in a polarizing microscope, as is demonstrated below by a mathematical model and confirming experimental evidence.

The linearly polarized beam from the gas laser source can be described by the Jones vector [5]

$$\begin{bmatrix} 1 \\ 0 \end{bmatrix}.$$

Manuscript received October 29, 1965; revised November 26, 1965. This work was supported by the Department of Defense's Joint Services Electronics Program (U. S. Army, U. S. Navy, and U. S. Air Force) under Grant AF-AFOSR-766-65.

The authors are with the Department of Electrical Engineering and Laboratories for Electronics and Related Science Research, The University of Texas, Austin, Texas.